

Ohmic resistance of solution in a vertical gas-evolving cell

M. P. M. G. WEIJS*, L. J. J. JANSSEN*, G. J. VISSER‡

Faculty of Chemical Technology* and Computing Centre‡, Eindhoven University of Technology, PO Box 513, 5600 MB Eindhoven, The Netherlands

Received 29 March 1996; revised 10 June 1996

Vertical electrolyzers with a narrow cell gap between a gas-evolving electrode and a membrane or diaphragm are used to produce industrial gases. Generally, the local current density decreases with height in the cell. Electrolyses are carried out with a KOH solution in a tall vertical divided rectangular cell with two gas-evolving electrodes. Either the hydrogen or the oxygen bubbles containing solution from the divided cell are passed through a small measuring cell. Ohmic resistance experiments are carried out in the small measuring cell with a gas-evolving electrode and a gas diffusion electrode, on which no gas bubbles are evolved. The effect of various parameters, viz. current density, solution flow rate and temperature, on the ohmic resistance of solution in the measuring cell are determined. It is found that the normalized ohmic resistance of the solution in the measuring cell during electrolysis increases with current density and with the gas voidage in the bulk of solution, decreases with increasing solution flow rate and is practically independent of temperature at 25 to 60°C. Moreover, it is found that for an oxygen evolving electrode in a solution containing only oxygen bubbles, as well as for a hydrogen evolving electrode in a solution containing only hydrogen bubbles, the normalized resistance of the solution between the gas-evolving electrode and the nongas evolving electrode is given by a relatively simple empirical relation. A relation is derived describing the gas voidage in the solution as a function of the distance from the gas-evolving electrode in the presence and the absence of gas bubbles in the bulk solution.

List of symbols

a_1	constant parameter in Equation 5 (mA^{-b_1})	r_∞	r at $i_m = 0$
a_2	constant parameter in Equation 7 (mA^{-b_2})	$r_{z,\text{cell}}$	normalized resistance for the cell at the height z
b_1	constant parameter in Equation 5	$r_{z,0,a}$	normalized resistance for the bubble boundary layer on the anode at $\epsilon_\infty = 0$ and at height z
b_2	constant parameter in Equations 6 and 7	$r_{z,0,c}$	normalized resistance for the bubble boundary layer on the cathode at $\epsilon_\infty = 0$ and at height z
d	distance (m)	$r_{0,\text{lim}}$	limiting value of r_0
d_{ac}	distance between the anode and the cathode in the measuring cell (m)	r_s	normalized specific surface resistivity, being R / R_p
I_{gp}	current in the gas-producing cell (A)	$r_{s,0}$	r_s at $I_{\text{gp}} = 0$
i	current density (kA m^{-2})	$r_{s,\infty}$	r_s at $i_m = 0$ and for uniform distribution of bubbles between the anode and the cathode in the measuring cell
i_m	current density in the measuring cell (kA m^{-2})	S_b	degree of screening of the electrode by attached bubbles
n_1	constant parameter in Equation 3	$S_{b,\text{lim}}$	limit value of S_b , to be approached at high current densities
Q_g	volumetric rate of gas saturated with water vapour ($\text{m}^3 \text{s}^{-1}$)	T	temperature (K)
Q_l	volumetric rate of liquid ($\text{m}^3 \text{s}^{-1}$)	v_l	linear velocity of liquid between the anode and the cathode in the measuring cell (m s^{-1})
R	ohmic resistance of solution between the anode and the cathode in the measuring cell (Ω)	x	distance from the electrode surface (m)
R_0	R at $I_{\text{gp}} = 0$ (Ω)	Z	impedance (Ω)
R_∞	R at $i_m = 0$ and for uniform distribution of bubbles between the anode and the cathode in the measuring cell (Ω)	Z'	real part of impedance (Ω)
R_p	ohmic resistance of the bubble-free solution between the anode and the cathode in the measuring cell (Ω)	Z''	imaginary part of impedance (Ω)
$R_{a,\text{av}}$	average radius of attached bubbles (m)	z	distance along the electrode from the leading edge of the electrode
$R_{a,\text{max}}$	maximum radius of attached bubbles (m)		
r	normalized (ohmic) resistance (Equation 4)		
r_0	r at $\epsilon_\infty = 0$ (Equation 2)		

Greek letters

β	gas volumetric flow ratio
δ	thickness of bubble boundary layer (m)
δ_0	δ at $\varepsilon_\infty = 0$ (m)
$\delta_{N,0}$	thickness of Nernst bubble layer at $\varepsilon_\infty = 0$ (m)
$\delta_{N,0,\text{lim}}$	limiting value of $\delta_{N,0}$
ε	voidage

ε_x	ε in bubble boundary layer at distance x
$\varepsilon_{x,0}$	ε at x and $\varepsilon_\infty = 0$
ε_{max}	maximum voidage
$\varepsilon_{0,0}$	ε at $x = 0$ and $\varepsilon_\infty = 0$
$\varepsilon_{0,\text{lim}}$	limit value of $\varepsilon_{0,0}$, to be approached at high current densities
ε_∞	ε in bulk of solution

1. Introduction

Vertical electrolyzers with parallel-plate electrodes are used industrially to produce gases such as chlorine, hydrogen and oxygen. The effect of gas-evolution on the ohmic resistance and the current distribution in these electrolyzers has been studied extensively to optimize cell design and operating electrolysis parameters like current density and flow rate. Moreover, knowledge of current distribution is of interest to the life of membranes and catalyst coatings.

An extensive review on current distribution in a vertical gas-evolving cell was published by Vogt [1]. To calculate the current distribution, the voidage distribution in a gas-evolving cell has to be known. This voidage and, therefore, the electrolyte resistivity, decreases with distance from the gas-evolving electrode and increases with height in the cell. Practically all models in vertical cells are based on a uniform gas voidage in the horizontal direction and an increasing gas voidage in the vertical direction [2–5]. Vogt [7] proposed a stagnant layer of finite thickness close to the gas evolving electrode from where bubbles protrude into a moving section, where the bubbles are uniformly distributed over the whole sectional area of the stagnant layer and also over that of the flowing section. The voidage in the stagnant layer is higher than that in the flowing section.

A bubble layer with a linear gas voidage profile – the Nernst bubble layer – adjacent to a gas-evolving electrode has been reported [6, 8], its thickness is a factor of about 10 larger than the average diameter of attached bubbles [8]. A model including a bubble layer adjacent to the gas-evolving electrode surface has been described [9]. Moreover, a correlation indicating the effect of the bulk solution voidage on the voidage at the gas-evolving electrode surface has been proposed [9].

Electrolysis of an alkaline electrolyte has been carried out in a vertical tall rectangular cell with a segmented oxygen and hydrogen-evolving electrode, where the ohmic resistance of the solution between two opposite segments, being a segment pair, has been determined as a function of current density, volumetric rate of liquid flow and gas voidage in the bulk of solution [9]. The increase in the ohmic resistance of solution is caused by the oxygen as well as the hydrogen-evolving electrode. In alkaline solution the behaviour of both types of bubbles is different; hydrogen bubbles do not coalesce as easily as oxygen bubbles [10].

To determine the effect of either the oxygen or the hydrogen-evolving electrode separately, experiments

have been carried out using a measuring cell with only one gas-evolving electrode where a gas-consuming electrode is used as counter electrode. A solution containing only one type of bubble, viz. hydrogen or oxygen bubbles, has been passed through the measuring cell. The purpose of this investigation is to determine the effect of gas voidage in the bulk solution on the gas voidage in the bubble layer for two different types of gas-evolving electrodes.

2. Experimental details*2.1. Measuring cell and gas-producing cell*

The experimental setup described in [11] was enlarged to two solution circuits and the undivided cell was replaced by a divided two-compartment electrolysis cell. A measuring cell, represented in Fig. 1, was placed in one of the two solution circuits between the outlet of the working electrode compartment of the electrolysis cell and the inlet of the solution reservoir overflow vessel. A thermometer was placed in the solution flow just after the outlet of the measuring cell.

The measuring cell had two different electrodes, that is, a working electrode made from 1 mm thick nickel plate and a gas-diffusion counter electrode (ECFG on Toray paper and 0.5 mg Pt cm⁻², E-TEK, USA). Two 1 mm thick Perspex sheets, 0.015 m in height and 0.030 m in width, were placed in the perforations of the nickel plate to obtain a flat cell wall including the working electrode. The nickel plate working electrode was 0.010 m in width and 0.020 m in height. The geometric electrode area, 0.010 m in width and 0.020 m in height, of the gas-diffusion counter electrode was adjusted by applying two coating layers 0.010 m in width and 0.015 m in height on the gas-diffusion electrode. The distance between

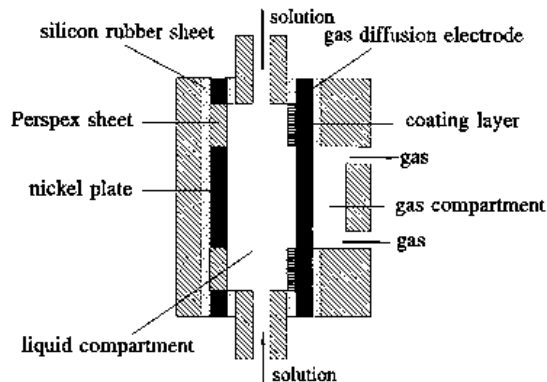


Fig. 1. Schematic plot of the measuring cell.

the electrodes was 4 mm. This distance was adjusted by placing a 3 mm thick Perspex liquid compartment frame with a hole of 0.010 m in width and of 0.050 m in length by sealing this frame with two silicon rubber sheets of 0.5 mm thickness. The cross-sectional area of the flow channel between the electrodes was 40 mm².

The parallel-plate gas-producing cell was a divided two-compartment Perspex cell; the compartments were separated by a cation-exchange membrane (Nafion[®], type 117). The solution in each compartment was pumped from a solution-reservoir overflow vessel upwards through the gap between membrane and electrode. Both electrodes were made from 0.1 mm thick platinum plate and were divided into 20 segments, each 0.010 m in width and 0.024 m in height, with a Perspex-filled length of 1 mm between successive segments. The distance between the electrodes and the membrane was 2 mm. This distance was adjusted by placing a 1 mm thick Perspex frame with a hole of 0.010 m in width and of 0.80 m in length by sealing this frame with two silicon rubber sheets of 0.5 mm thickness. The cross-sectional area of the flow channel between the electrodes and the membrane was 20 mm².

2.2. Electrical measurements

The potential difference between each pair of electrode segments in the parallel-plate gas-producing cell was adjusted by a special constant-voltage source with 20 independent channels (GEEST-2). Each segment was connected to the constant-voltage source by two contacts, one for the power supply and the other for the control of the potential. The potential range of the constant voltage source could be varied between 0 and 50 V and the maximum current load for a pair of segments was 2.5 A.

The impedance measurements were carried out with a Solartron 1250 frequency response analyser and a Solartron electrochemical interface 1286, controlled by an Olivetti personal computer M24 and the EISDATA software package (EISDATA v2.40, J. Schramm, TU Delft, The Netherlands (1989–90)). The interface was used in the galvanostatic mode, where a controlled direct current was driven through the electrodes in the measuring cell. The impedance of the measuring cell was determined in the frequency range from 65500 to 50000 Hz. In this frequency range the real part of impedance was practically constant and the imaginary part was approximately zero.

2.3. Electrolysis conditions

Experiments were carried out with average current densities in the measuring cell up to 2.5 kA m⁻² using a 12 wt% KOH solution at temperatures between 298 and 333 K, mostly at 323 K. The total current through the parallel-plate gas-evolving cell was varied between 0 and 21 A, where all segments were charged.

The volumetric rate of solution flow was varied between 2×10^{-6} and 12×10^{-6} m³ s⁻¹.

The temperature was measured during each experiment. A small increase in temperature, maximum 2°C under the most extreme conditions applied, was found. The effect of the temperature deviation was taken into account, so that the results for a series of experiments could be given for the same temperature.

3. Results

3.1. Introduction

The alternating current impedance technique is widely used to determine the ohmic resistance of the solution in an electrochemical cell. This technique is well described in [12]. The impedance of the measuring cell consisting of a gas-evolving and gas-consuming electrode and the solution in between was measured. It was found that in the high-frequency range from 65 500 to 50 000 Hz Z'' was practically zero and Z' fluctuated, significantly, because of fluctuations in the gas bubble formation of the gas-evolution. It is likely that the average Z' in the considered frequency range is equal to the ohmic resistance of the solution in the measuring cell, R .

3.2. Ohmic resistance in the absence of bubbles in the bulk of solution

The ohmic resistance of the solution in the measuring cell in the absence of bubbles evolved by the gas-producing cell, R_0 was determined at various current densities in the measuring cell, i_m . It was found that the ohmic resistance R_0 increases with increasing current density i_m . The intersection of the R_0/i_m curve with the R_0 axis gives R_p , being R_0 in the absence of gas evolution.

In Fig. 2 the normalized resistance r_0 , being R_0/R_p , is plotted as a function of i_m for oxygen and hydrogen evolution at various liquid flow rates. r_0 increases at a steadily decreasing rate with increasing i_m , decreases with increasing rate of solution flow and depends on the nature of the gas evolved. Moreover, for both types of gas evolved at low solution flow rates r_0 approaches a limiting value, viz. $r_{0,\text{lim}}$. Using the results from Fig. 2 $(r_0-1)/(r_{0,\text{lim}}-r_0)$ was plotted against i_m on a double logarithmic scale, where a value for $r_{0,\text{lim}}$ had been chosen to obtain a straight line for the whole range of i_m . It was found that for oxygen $r_{0,\text{lim}} = 3.3$ and $(r_0-1)/(r_{0,\text{lim}}-r_0)$ was proportional to $i_m^{1.13}$ and for hydrogen $r_{0,\text{lim}} = 2.0$ and $(r_0-1)/(r_{0,\text{lim}}-r_0)$ was proportional to $i_m^{1.07}$.

3.3. Ohmic resistance in the presence of bubbles in bulk solution

The ohmic resistance of the solution in the measuring cell was determined at various current densities in the measuring cell and at various currents in the gas-

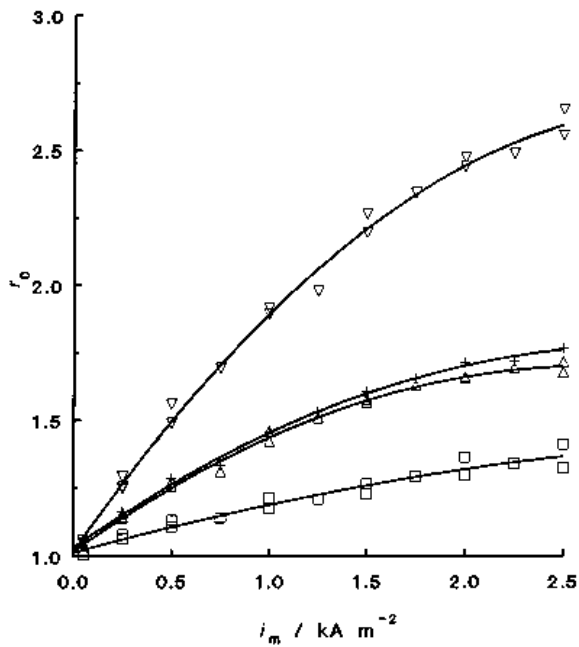


Fig. 2. The normalized resistance r_0 as a function of the current density i_m for oxygen and hydrogen evolution at various Q_1 . (\square) hydrogen, $11 \times 10^{-6} \text{ m}^3 \text{ s}^{-1}$; (+) hydrogen, $3 \times 10^{-6} \text{ m}^3 \text{ s}^{-1}$; (\triangle) hydrogen, $2 \times 10^{-6} \text{ m}^3 \text{ s}^{-1}$; (∇) oxygen, $3 \times 10^{-6} \text{ m}^3 \text{ s}^{-1}$.

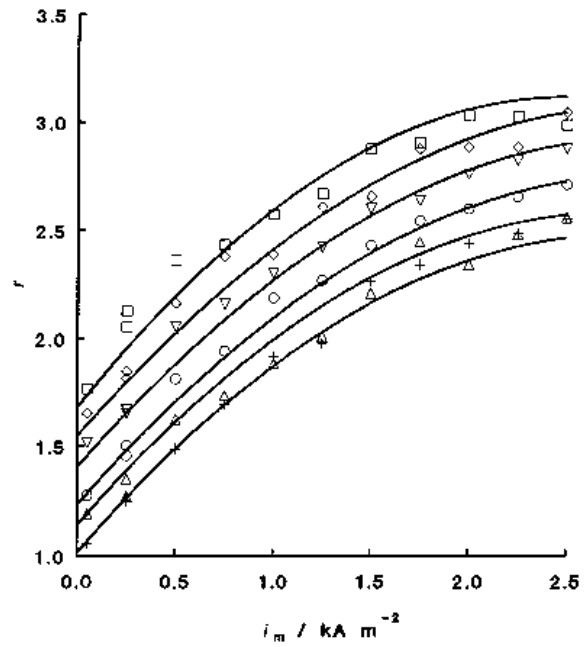


Fig. 4. The normalized resistance r as a function of the current density i_m for oxygen evolution at various I_{gp} and at $Q_1 = 3 \times 10^{-6} \text{ m}^3 \text{ s}^{-1}$. I_{gp} : (+) 0, (\triangle) 3, (\circ) 6, (∇) 9, (\diamond) 12 and (\square) 15 A.

producing cell. The latter variation corresponds to a variation in the gas voidage in the bulk of the solution passing through the measuring cell.

If Figs 3 and 4 the normalized resistance r , being R/R_p , for hydrogen as well as for oxygen evolution, is plotted as a function of i_m for various I_{gp} , where all the segments in the gas-producing cell were charged. The data at high gas evolution rate show a considerable scatter due to fluctuations in the solution gas voidage. Moreover, it was found that pretreat-

ment of the electrode affects the normalized resistance r . Figures 3 and 4 show that r/i_m curves are bent and are almost parallel to one another for hydrogen and oxygen evolution.

The normalized resistance r for oxygen and hydrogen evolution was also determined for two series of experiments with a constant current density in the measuring cell and a varying current in the gas-producing cell. In Figs 5 and 6 the normalized resistance r is plotted as function of I_{gp} for hydrogen and oxy-

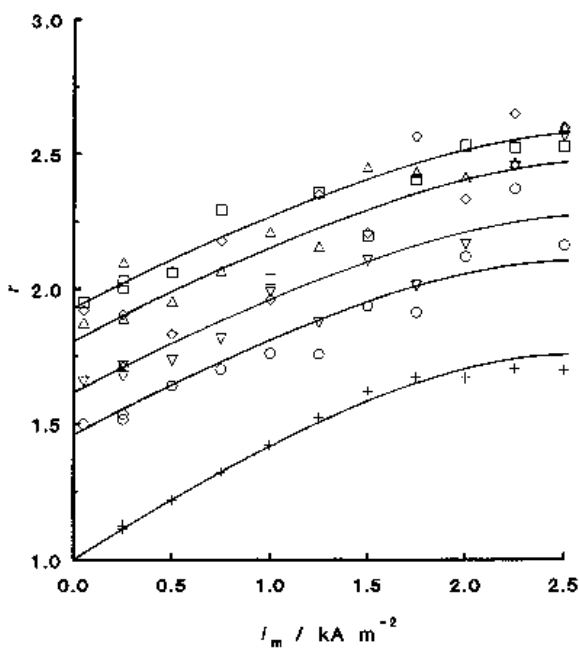


Fig. 3. The normalized resistance r as a function of the current density i_m for hydrogen evolution at various I_{gp} and at $Q_1 = 3 \times 10^{-6} \text{ m}^3 \text{ s}^{-1}$. I_{gp} : (+) 0, (\circ) 6, (∇) 9, (\diamond) 12, (\square) 15 and (\triangle) 18 A.

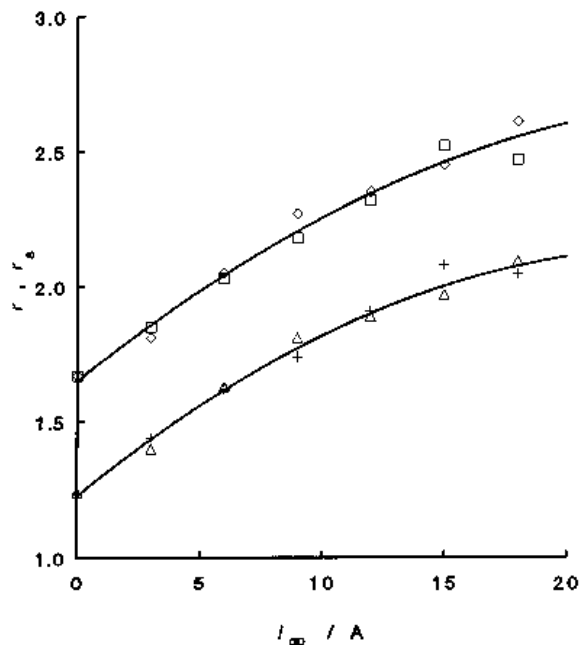


Fig. 5. The normalized resistance r (+ and \square) and the calculated reduced specific surface resistivity r_s (\triangle and \diamond) as a function of the current I_{gp} for hydrogen evolution at two different i_m and at $Q_1 = 3 \times 10^{-6} \text{ m}^3 \text{ s}^{-1}$. (+, \triangle) 0.5 and (\square , \diamond) 2 kA m^{-2} .

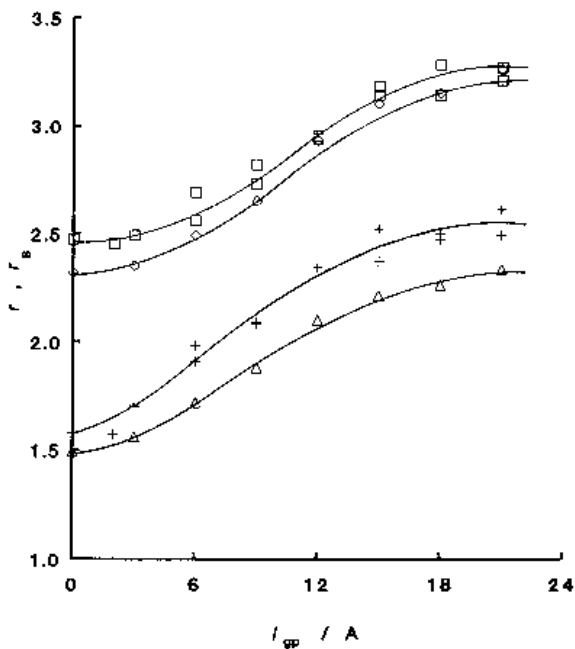


Fig. 6. The normalized resistance r (+ and \square) and the calculated reduced specific surface resistivity r_s (\triangle and \diamond) as a function of the current I_{gp} for oxygen evolution at two different i_m and at $Q_1 = 3 \times 10^{-6} \text{ m}^3 \text{ s}^{-1}$. (+, \triangle) 0.5 and (\square , \diamond) 2 kA m^{-2} .

gen evolution, respectively. Figures 5 and 6 show that the r/I_{gp} curves in each figure are slightly bent and almost parallel to one another.

3.4. Effect of linear velocity of liquid

The effect of the linear velocity of the liquid was investigated by performing a series of experiments at various liquid flow rates for hydrogen and oxygen evolution. The ohmic resistance of the solution in the measuring cell, R , was determined at two different measuring cell current densities, viz. 0.5 and 2 kA m^{-2} , and with a current of practically zero in the gas-producing cell. R_p was obtained from R at $i_m = 0.5 \text{ kA m}^{-2}$ by extrapolation, as applied for r in Figs 3 and 4.

In Fig. 7 $\log(r_0 - 1)$ is plotted as a function of the linear velocity of the liquid v_1 for hydrogen and oxygen evolution. From Fig. 7 it follows that all curves are parallel to one another and that $r_0 - 1$ is proportional to $\exp(-2.7 v_1)$ for hydrogen and oxygen evolution.

3.5. Effect of temperature

The effect of temperature was investigated by performing a series of experiments at various temperatures for hydrogen and oxygen evolution. R_p at 323 K was obtained as described in 3.4. From this R_p and using the temperature dependence of the conductivity of a 2 M KOH solution, R_p at other temperatures was calculated. The normalized resistance of the solution in the measuring cell was determined at two different current densities in the measuring cell and with a current of practically zero in the gas-producing cell.

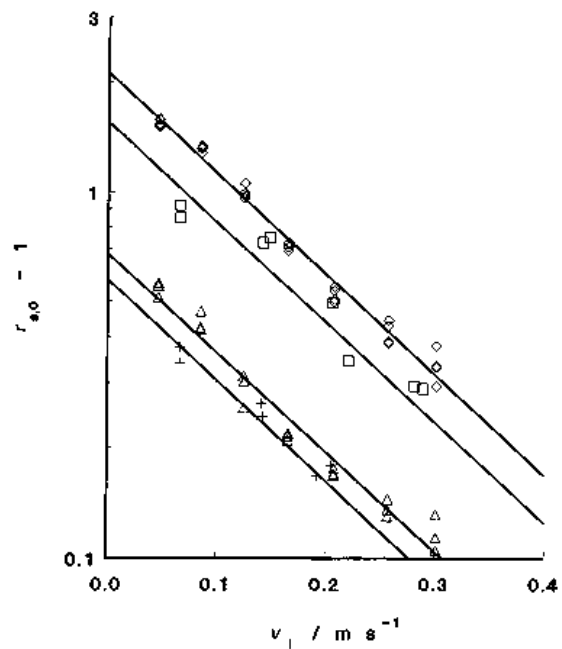


Fig. 7. The normalized resistance increment $r_0 - 1$ is plotted as a function of the linear velocity of the liquid v_1 in the measuring cell at the leading edge of the electrode for oxygen and hydrogen evolution at various i_m . (+) hydrogen, 0.5 kA m^{-2} , (\square) hydrogen, 2 kA m^{-2} , (\triangle) oxygen, 0.5 and (\diamond) oxygen, 2 kA m^{-2} .

The experiments for hydrogen evolution were carried out at increasing and decreasing temperature while the experiments for oxygen evolution were carried out for increasing temperature only.

In Fig. 8 the normalized resistance r_0 is plotted as a function of temperature T for hydrogen and oxygen evolution at $i_m = 0.5$ and 2 kA m^{-2} . Figure 8 shows that r_0 increases with increasing temperature. This

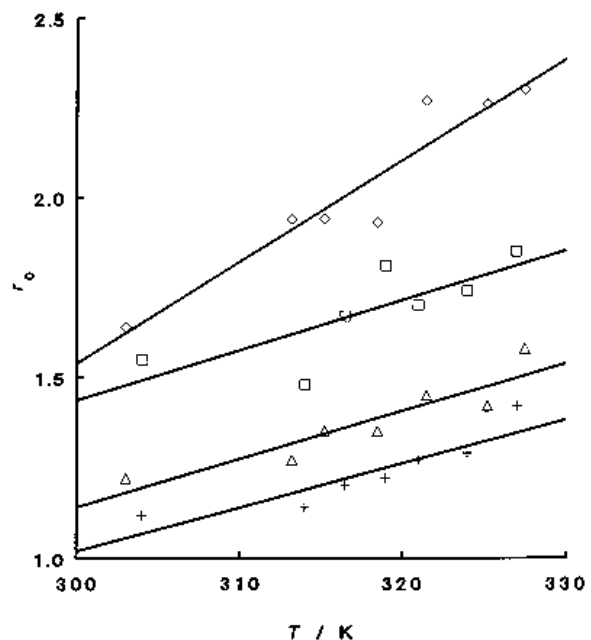


Fig. 8. The normalized resistance r_0 as a function of the temperature T at the outlet of the measuring cell for oxygen and hydrogen evolution at various i_m and at $Q_1 = 3 \times 10^{-6} \text{ m}^3 \text{ s}^{-1}$. (+) hydrogen, 0.5 kA m^{-2} ; (\square) hydrogen, 2 kA m^{-2} ; (\triangle) oxygen, 0.5 kA m^{-2} ; (\diamond) oxygen, 2 kA m^{-2} .

increase in r_0 is caused by an increase in the water vapour pressure of a 2 M KOH solution with increasing temperature. The volumetric rate of evolved gas saturated with water vapour at a constant current density increases strongly with temperature.

4. Theory

To calculate the ohmic resistance of the solution in a gas-evolving cell, a model including a bubble boundary layer adjacent to the surface of the gas-evolving electrode has been presented by Bongenaar-Schlenter [7, 8]. This model, with related assumptions, is presented in [9].

The voidage in the bubble boundary layer in the absence of bubbles in the bulk of solution is given by

$$\varepsilon_{x,0} = \varepsilon_{0,0} - \frac{\varepsilon_{0,0}x}{\delta_{N,0}} \quad (1)$$

where $\delta_{N,0}$ is the thickness of the Nernst bubble layer at $\varepsilon_\infty = 0$ and $\varepsilon_{0,0}$ is the voidage at $x = 0$ and $\varepsilon_\infty = 0$.

The reduced specific surface resistivity is given by

$$r_{s,0} = \frac{1}{d_{ac}} \int_0^{\delta_{N,0}} (1 - \varepsilon_{x,0})^{-1.5} dx + \left(\frac{d_{ac} - \delta_{N,0}}{d_{ac}} \right) \quad (2)$$

where the first term is related to the Nernst bubble layer and the second term to the bubble-free solution between the Nernst bubble layer and the nongas-evolving counter electrode. Numerical calculations for various $\delta_{N,0}$, $\varepsilon_{0,0}$ and d_{ac} have been carried out [9].

Even in the presence of bubbles in the bulk solution a bubble boundary layer at the surface of the gas-evolving electrode exists. The voidage in the bulk solution, ε_∞ , affects the voidage in the bubble boundary layer, ε_x , as well as the thickness of the bubble boundary layer, δ . To describe this effect a general correlation has been proposed viz.

$$\varepsilon_x^{m_1} = \varepsilon_{0,0}^{m_1} \left(1 - \frac{x}{\delta_{N,0}} \right)^{m_1} + \varepsilon_\infty^{m_1} \quad (3)$$

It can be shown that the reduced specific surface resistivity at various ε_∞ is given by [9]

$$r_s = \frac{1}{d_{ac}} \int_0^{\delta_{N,0}} (1 - \varepsilon_x)^{-1.5} dx + (1 - \varepsilon_\infty)^{-1.5} \left(\frac{d_{ac} - \delta_{N,0}}{d_{ac}} \right) \quad (4)$$

5. Discussion

5.1. Bubble boundary layer in the absence of bubbles in bulk of solution

During the electrolysis of a KOH solution a bubble boundary layer is formed at the transparent hydrogen-evolving cathode and at the transparent oxygen-evolving anode [6–8, 13]. The occurrence of a bubble boundary layer is well-known in boiling heat transfer [14].

A supersaturated liquid layer exists next to the wall of a gas-evolving electrode, while the bulk liquid may be saturated. Bubbles nucleate on the surface of the gas-evolving electrode and grow in the supersaturated liquid layer adjacent to the surface [6]. The supersaturated liquid layer contains bubbles of all ages, either still attached or detached bubbles carried along with the two-phase flow. The bubbles are in the process of growing and/or of coalescing.

Sillen [6] has reported pictures showing the bubble-containing boundary layer at both hydrogen-evolving cathode and oxygen-evolving anode in 1 M KOH. Its thickness, δ_0 , increases with increasing current density for gas-evolution and increasing distance z along the electrode from the leading edge and decreases with increasing flow rate. From [6] it follows that the effect of the height and the flow rate on δ_0 are practically independent of the nature of the gas evolved and are given by the relationships $\delta_0 \sim z^{0.7}$ and $\delta_0 \sim v_1^{0.18}$. However the effect of current density on δ_0 depends strongly on the nature of the gas evolved. Assuming $\delta_{N,0}$ is proportional to δ_0 , it follows [6] that

$$\delta_{N,0} = a_1 i^{b_1} \quad (5)$$

where $b_1 = 0.40$ for hydrogen and 0.75 for oxygen.

The degree of screening of the gas-evolving electrode by the attached bubbles, S_b , is given in [6, 13] at various current densities, flow rates, gas pressures and KOH concentrations for hydrogen-evolving and oxygen-evolving electrodes. The degree of screening, S_b , is the fraction of the electrode surface covered by the projection of the attached bubbles. It has been found that

$$S_b / (S_{b,\text{lim}} - S_b) \sim i^{b_2} \quad (6)$$

where $b_2 = 1.34$ using $S_{b,\text{lim}} = 0.60$ for both the hydrogen-evolving and the oxygen-evolving electrode in 1 M KOH and in free and forced convection [6].

From elementary geometric considerations for various lattice types of bubble arrangement it has been calculated that, for bubbles of uniform size, ε_{max} , ranges from 0.52 for cubic lattice to 0.74 for a tetrahedral lattice [15]. However, since the size of bubbles shows a large spread, it can be shown that ε_{max} can reach larger values than those mentioned above. For milled alumina packings of continuous size distribution it was determined that the packing fraction is about 0.62 [16]. The packing fraction is similar to the void fraction for a bubble-containing solution.

To calculate the increase in the ohmic resistance of solution due to gas-evolution it is reasonable to assume that the voidage decreases continuously with increasing x and that the voidage at $x = 0$, $\varepsilon_{0,0}$, is the largest. Moreover, it is assumed that $\varepsilon_{0,0}$ is proportional to S_b and $\varepsilon_{0,\text{lim}}$ to $S_{b,\text{lim}}$. Consequently,

$$S_b / (S_{b,\text{lim}} - S_b) = \varepsilon_{0,0} / (\varepsilon_{0,\text{lim}} - \varepsilon_{0,0}) = a_2 i^{b_2} \quad (7)$$

From the experimental results given in [13] it was found that b_2 and $S_{b,\text{lim}}$ are related to each other. Assuming $S_{b,\text{lim}}$ to be 0.60, 0.65 or 1.0 corresponding

to the same values for $\epsilon_{0,\text{lim}}$ it was found that b_2 is 1.34, 1.25 or 1.12

Using Equations 1 and 2 and $d_{\text{ac}} = 4 \times 10^{-3}$ m the normalized ohmic resistivity has been calculated for the above mentioned sets for b_2 and $\epsilon_{0,\text{lim}}$ and for a wide range of a_2 , a_1 and b_1 . The calculated normalized ohmic resistivities have been compared with the experimental ones for the series of experiments given in Fig. 2. Curve fitting was done by varying the parameters one by one, utilizing the method of linear search. As minimization criterion the sum of the squared differences between the theoretical and measured data was used. It was found that the best fit was obtained for $\epsilon_{0,\text{lim}} = 0.65$ and $b_2 = 1.25$ and moreover, the effect of b_2 in the same range from 0.8 to 1.4 on the obtained results for a_2 , a_1 and b_1 is negligible. Calculations showed that, assuming $b_2 = 1.25$ and $\epsilon_{0,\text{lim}} = 0.65$, for the hydrogen-evolving electrode the parameter b_1 is practically independent of the flow rate, viz. $b_1 = 0.39 \pm 0.02$, and the parameter a_1 decreases and a_2 increases with increasing flow rate, viz. $a_1 = 0.0020, 0.0020$ and 0.0010 m and $a_2 = 8.4, 7.8$ and 5.3 for $v_1 = 0.042, 0.075$ and 0.28 m s $^{-1}$, respectively, where i is in kA m $^{-2}$.

For oxygen-evolving electrodes two series of experiments were carried out at the same flow rate. Assuming $b_2 = 1.25$ and $\epsilon_{0,\text{lim}} = 0.65$, it was calculated that $b_1 = 0.67$, $a_1 = 0.0030$ m and $a_2 = 82$.

Section 3.2 shows that $r_{0,\text{lim}}$ is 2.0 and 3.3 for a hydrogen and an oxygen evolving electrode, respectively. Assuming $\epsilon_{0,\text{lim}} = 0.65$ and using Equation 2, it was calculated that $\delta_{0,\text{N},\text{lim}} = 3.6 \times 10^{-3}$ m and 8.2×10^{-3} m for, respectively a hydrogen and an oxygen evolving electrode. It is well known that the nature of gas evolution depends on its rate and that a transition from bubble to film electrolysis occurs at very high rate of gas production [1]. It is likely that $\epsilon_{0,\text{lim}}$ and $\delta_{\text{N},0,\text{lim}}$ will approach limiting values for bubble electrolysis. $\delta_{\text{N},0,\text{lim}}$ for oxygen evolution is larger than that for hydrogen evolution, probably due to a difference in adhesion strength between bubbles and electrode surface.

In Fig. 9 calculated values of $\epsilon_{0,0}$ and $\delta_{\text{N},0}$ are plotted against current density for a hydrogen-evolving electrode at $v_1 = 0.28$ m s $^{-1}$ corresponding to $Q_1 = 11 \times 10^{-6}$ m 3 s $^{-1}$ and an oxygen-evolving electrode at $v_1 = 0.075$ m s $^{-1}$ corresponding to $Q_1 = 3 \times 10^{-6}$ m 3 s $^{-1}$. It follows that for the hydrogen-evolving electrode $\epsilon_{0,0}$ and $\delta_{\text{N},0}$ increase strongly with increasing current density and for the oxygen-evolving electrode $\epsilon_{0,0}$ is almost equal to $\epsilon_{0,\text{lim}}$ for $i > 0.25$ kA m $^{-2}$ and $\delta_{\text{N},0}$ increases strongly with increasing current density.

5.2. Effect of the bulk of solution voidage on bubble boundary layer voidage

The measuring cell was fed with an alkaline solution containing either hydrogen or oxygen bubbles. Assuming a uniform distribution of bubbles in the solution between the electrodes in the measuring cell,

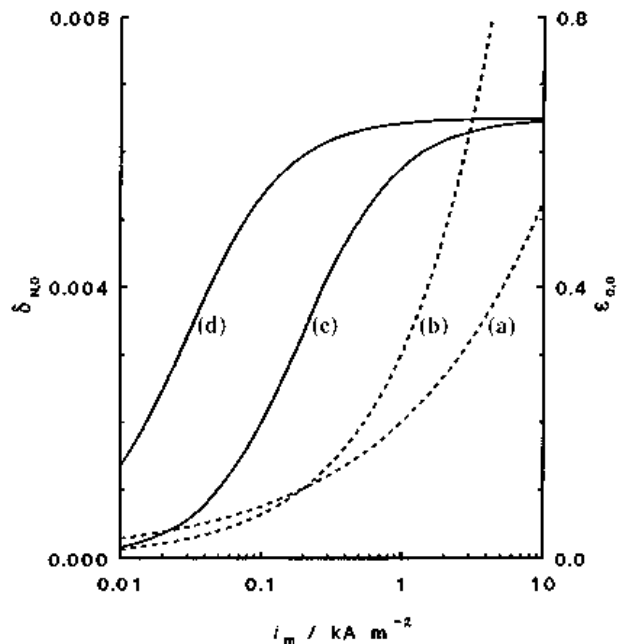


Fig. 9. The calculated thickness of Nernst bubble layer $\delta_{\text{N},0}$ and the calculated voidage at the electrode surface $\epsilon_{0,0}$ as a function of the current density i_m on a logarithmic scale for oxygen and hydrogen evolution at $Q_1 = 3 \times 10^{-6}$ m 3 s $^{-1}$. (a) $\delta_{\text{N},0}$, hydrogen; (b) $\delta_{\text{N},0}$, oxygen; (c) $\epsilon_{0,0}$, hydrogen; (d) $\epsilon_{0,0}$, oxygen.

the bulk solution voidage can be calculated via the Bruggeman equation, viz.

$$r_\infty = (1 - \epsilon_\infty)^{-3/2} \quad (8)$$

It was found that for both the hydrogen and the oxygen bubble-containing solution ϵ_∞ increases continuously with increasing I_{gp} and decreasing Q_1 . Moreover, ϵ_∞ at $\beta < 0.3$ is practically equal to the gas volumetric flow ratio β , being $Q_g/(Q_g + Q_1)$, and the difference $\beta - \epsilon_\infty$ at $\beta > 0.3$ increases more and more with increasing I_{gp} . The large difference $\beta - \epsilon_\infty$ at $\beta > 0.3$ is caused by bubble coalescence which occurs more frequently with increasing voidage and enlarges bubble size and also the bubble-slip ratio.

Figures 3 and 4 show that for the hydrogen-evolving, as well as the oxygen-evolving, cell r/i_m curves at various I_{gp} are practically parallel to one another. This parallelism was also obtained for the r/I_{gp} curves at $i_m = 0.5$ and 2 kA m $^{-2}$ (Fig. 5). Equation 4 gives the normalized resistivity for a cell with only one gas-evolving electrode and fed with a bubble-containing solution. The voidage of this solution depends on various parameters, for instance, the current I_{gp} , the solution flow rate and the nature of the gas evolved.

The normalized specific surface resistivity, r_s , was calculated as a function of ϵ_∞ for various n_1 , $\epsilon_{0,0}$ and $\delta_{\text{N},0}$. Numerical results are presented in [17]. It is found that the r_s/ϵ_∞ curves and the $r_s/\epsilon_{0,0}$ curves diverge for $n_1 = 1$, are parallel to one another for $n_1 = 2$ and converge for $n_1 = 3$ and 4 [17]. From the parallelism of the experimental r/i_m curves at various I_{gp} (Figs 3, 4) and the parallelism of the experimental r/I_{gp} curves at two different i_m (Figs 5 and 6) it follows that $n_1 = 2$. This means that the voidage in the bubble

boundary layer with a thickness $\delta_{N,0}$ at the gas-evolving electrode is given by

$$\varepsilon_x^2 = \varepsilon_{0,0}^2 \left(1 - \frac{x}{\delta_{N,0}}\right)^2 + \varepsilon_\infty^2 \quad (9)$$

This relation was also obtained for a vertical undivided cell where a solution of 1.5 kmol m^{-3} NaCl at pH 9 was electrolysed. In this cell hydrogen bubbles were evolved on a segmented titanium cathode and hypochlorite was formed by hydrolysis of chlorine initially produced on the anode [17]. This hypochlorite generating cell can be considered more or less as a cell with one gas-evolving electrode, since the evolution of chlorine and/or oxygen bubbles can be disregarded. From the experimental results with an undivided vertical cell with two gas-evolving electrodes, viz oxygen-evolving and hydrogen-evolving electrodes, it was concluded that $n_1 = 4$. This conclusion was based on the results given in Fig. 4 from [9]. It was already mentioned that the normalized resistivity at small measuring currents given in Fig. 4 from [9] was effected by the current loading of the gas-producing electrode. This effect is noticeable over a wider range of measuring current than assumed in [9]. Taking this into account, it may be shown that the results can be reasonably described with $n_1 = 2$.

From Equation 9 it follows that the voidage profile in the bubble boundary layer becomes curved due to the effect of the bulk solution voidage. The normalized specific surface resistivity for hydrogen and oxygen evolution was calculated as a function of I_{gp} at $i_m = 0.5$ and 2 kA m^{-2} using Equation 4, $d_{ac} = 4 \times 10^{-3} \text{ m}$, $\delta_{N,0}$ calculated with a_1 and b_1 , $\varepsilon_{0,0}$ calculated with a_2 and b_2 , $\varepsilon_{0,lim} = 0.65$ and ε_∞ from r_∞ . The calculated r_s for $n_1 = 2$ are given in Figs 5 and 6 for a hydrogen-evolving and an oxygen-evolving electrode, respectively. Calculations were carried out for $n_1 = 1$ and 3. In particular, the differences between the calculated and experimental results are very large for $n_1 = 1$. The best agreement is obtained for $n_1 = 2$. From Figs 5 and 6 it follows that the agreement between the calculated r_s and experimental r is good.

Moreover this research has delivered a very simple empirical relation to calculate the normalized resistance as a function of the height in a cell with one

gas-evolving electrode, if the gas bubbles formed in the lower part of the cell are uniformly distributed across the cross-section of the cell. This relation can be written by

$$r_{z,cell} = r_{z,0} + r_{z,\infty} - 1 \quad (10)$$

Using the same assumption about the distribution of gas bubbles, a similar relation can be proposed for an undivided cell with two gas-evolving electrodes, cathode and anode, viz.

$$r_{z,cell} = r_{z,0,a} + r_{z,0,c} + r_{z,\infty} - 1 \quad (11)$$

Also, for cells with two gas-evolving electrodes separated by a membrane or diaphragm relations for $r_{z,cell}$ can be derived. Relations for $r_{z,cell}$ can be very helpful in calculating the current distribution in and to optimize the design of gas-evolving cells.

References

- [1] H. Vogt, in 'Comprehensive Treatise of Electrochemistry', vol. 6 (edited by E. Yeager, J. O'M. Bockris, B. E. Conway and S. Sarangapani), Plenum Press, New York (1983) p. 476.
- [2] C. W. Tobias, *J. Electrochem. Soc.* **106** (1959) 833.
- [3] A. D. Martin and A. A. Wragg, *J. Appl. Electrochem.* **14** (1984) 653.
- [4] J. M. Bisang, *ibid.* **21** (1991) 760.
- [5] M. Kuhn and G. Kreysa, *J. Appl. Electrochem.* **19** (1989) 720.
- [6] C. W. M. P. Sillen, PhD thesis, Eindhoven University of Technology, Eindhoven (1983).
- [7] H. Vogt, *Electrochim. Acta* **9** (1981) 1311.
- [8] B. E. Bongenaar-Schlenter, L. J. J. Janssen, S. J. D. van Stralen and E. Barendrecht, *J. Appl. Electrochem.* **15** (1985) 537.
- [9] L. J. J. Janssen and G. J. Visser, *ibid.* **21** (1991) 386.
- [10] L. J. J. Janssen and E. Barendrecht, *Electrochim. Acta* **30** (1985) 683.
- [11] L. R. Czarnetzki and L. J. J. Janssen, *J. Appl. Electrochem.* **19** (1989) 630.
- [12] R. Greef, R. Peat, L. M. Peter, D. Pletcher and J. Robinson, 'Instrumental Methods in Electrochemistry', Ellis Horwood, Chichester (1986).
- [13] L. J. J. Janssen, C. W. M. P. Sillen, E. Barendrecht and S. J. D. van Stralen, *Electrochim. Acta* **29** (1984) 633.
- [14] L. S. Tong, 'Boiling Heat Transfer and Two-phase Flow', John Wiley & Sons, New York (1965).
- [15] G. Kreysa and M. Kuhn, *J. Appl. Electrochem.* **15** (1985) 517.
- [16] J. S. Reed, 'Introduction to the Principles of Ceramic Processing', Wiley-Interscience, Chichester (1988) ch.13, p. 191.
- [17] L. R. Czarnetzki, PhD thesis, Eindhoven University of Technology, Eindhoven (1989).